

Elucidating the role of an Ir insertion layer in mediating interfacial perpendicular anisotropy, Dzyaloshinskii-Moriya interaction, and spin-orbit torque in Pt/Ir/Co

Haodong Fan,¹ Ziji Shao,¹ Jiale Wang,¹ Menghao Jin,¹ Birui Wu,¹ Zhongshu Feng,¹ Mingzhang Wei,¹ Changqiu Yu,¹ Jiahong Wen,¹ Hai Li,¹ Tingwei Chen,² Bo Liu,² Wenjun Li,^{1,*} and Tiejun Zhou^{1,2,†}

¹*School of Electronics and Information, Hangzhou Dianzi University, Hangzhou, Zhejiang 310018, China*

²*Key Laboratory of Spintronics Materials, Devices and Systems of Zhejiang Province, Zhejiang 311305, China*



(Received 1 October 2023; accepted 20 November 2023; published 6 December 2023)

The advancement of spin-orbit torque (SOT)-based spintronic devices hinges on the ability to optimize interfacial spin-orbit coupling phenomena. This work elucidates the modulation of key spintronic parameters by inserting an Ir layer at Pt/Co and PtCr/Pt(0.5)/Co interfaces. A comprehensive investigation into the thickness-dependent perpendicular magnetic anisotropy, Dzyaloshinskii-Moriya interaction, spin-orbit torque efficiency, and switching current density is undertaken. The results reveal that an ultrathin 0.1 nm Ir insertion layer can enhance the dampinglike SOT efficiency by over 26% in Pt/Co and 10% in PtCr/Co systems, attributed to increased interfacial impurity scattering. Strikingly, the magnetic anisotropy and Dzyaloshinskii-Moriya interaction exhibit a nonmonotonic relationship with Ir thickness, minimized at 0.4–0.5 nm, explained by interfacial roughness effects evidenced through first-principles calculations. The critical switching current density becomes widely tunable from $1.6\text{--}3.5 \times 10^7$ (A/cm²) in Pt/Ir/Co and $1.0\text{--}2.0 \times 10^7$ (A/cm²) in PtCr/Ir/Co, respectively, reduced by nearly 50% with a 0.4 nm Ir insertion. These findings provide significant physical insights into interfacial spin-orbit coupling mechanisms and interface engineering of spintronic devices using insertion layers. The capability to substantially increase SOT efficiency while reducing the switching current highlights the promise of an Ir insertion layer to unlock the full potential of SOT-MRAM technology.

DOI: [10.1103/PhysRevB.108.224409](https://doi.org/10.1103/PhysRevB.108.224409)

I. INTRODUCTION

Spin-orbit torque (SOT) has emerged as a promising spintronic technology, owing to advantages in energy efficiency, nonvolatility, speed, and integration density [1–4]. Extensive research has validated SOT as an effective approach to manipulate magnetization [5–7], drive dynamics of domain [8,9], and skyrmion [10], by converting charge current to spin current through the spin Hall effect [11,12] or Rashba-Edelstein effect [13,14]. A key goal for SOT-based magnetoresistive random access memory (MRAM) is concurrent optimization of charge-to-spin conversion efficiency (for storage density) and electrical resistivity (for power), despite there being intrinsic tradeoffs between them [15].

A pivotal technique is interface engineering of the heavy-metal (HM)/ferromagnet (FM) bilayer, e.g., by inserting a spacer layer, which enables modulation of crucial properties including perpendicular magnetic anisotropy (PMA), SOT efficiency, critical switching current density, and interfacial Dzyaloshinskii-Moriya interaction (DMI) [16,17]. This is attributed to the intricate spin-dependent interfacial phenomena: spin angular momentum transfer, spin accumulation, spin memory loss, and spin backflow [18,19]. For instance, a NiO

layer at the Pt/CoFeB interface reduces spin memory loss and enhances SOT efficiency [18]; metallic Hf or Au interlayers improve SOT via reduced spin mixing conductance or increased spin transmission [20,21].

The strong spin-orbit coupled (SOC) 5d metal Ir is promising for spintronics, with Pt/Co/Ir exhibiting substantial DMI for skyrmionics [22–24], IrMn enabling exchange bias and field-free switching [25–27], and Ir providing antiferromagnetic coupling for synthetic antiferromagnets [28–31]. Therefore, it is imperative to conduct a systematic analysis on the SOT interface modulation in HM/Ir/FM trilayers. So far, only magnetoresistance modulation in Ta/Ir/CoFeB [32], both SOT efficiency and PMA optimization in W/Ir/CoFeB have been demonstrated [19]. Nevertheless, the modulation of PMA, SOT efficiency and DMI in Pt/Ir/Co remains unexplored, especially Ir insertion may benefit SOT performance.

Here, the thickness-dependent PMA, SOT efficiency, DMI effective field, and switching current density in Pt/Ir/Co and PtCr/Ir/Co are systematically investigated. Hysteresis loop shift reveals that an ultrathin 0.1 nm Ir insertion layer can enhance the dampinglike SOT efficiency by over 26% in Pt/Co and 10% in PtCr/Co systems, which can be due to additional interfacial impurity scattering. The minimum value of the PMA field and DMI effective field that arises at $t_{\text{Ir}} = 0.4$ nm can be attributed to the interfacial roughness, where the Pt/Co interface is severely disrupted, yet a perfect Ir/Co interface cannot be formed, as evidenced by combined high-temperature sputtering-induced PMA enhancement proofs and the first-principles calculations. Besides, DMI exchange

* Author to whom correspondence should be addressed: liwenjun@hdu.edu.cn

† Author to whom correspondence should be addressed: tjzhou@hdu.edu.cn

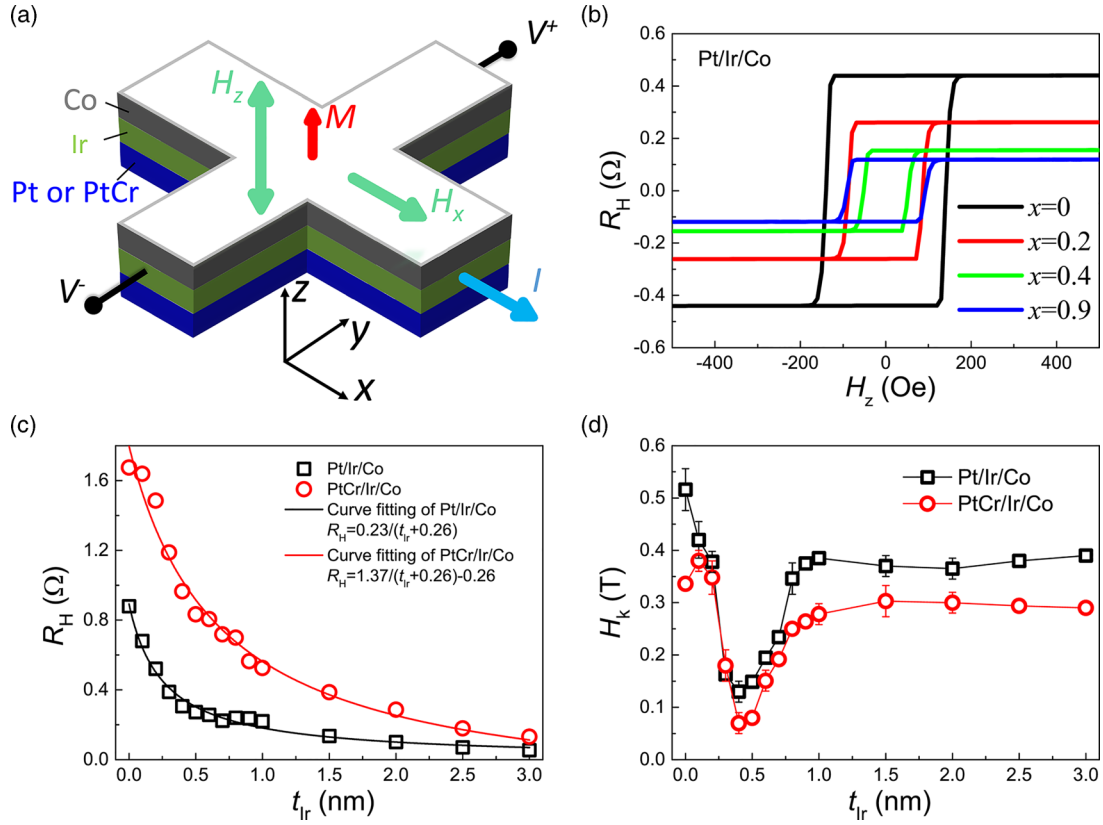


FIG. 1. (a) The schematic diagram of the measurement scheme for Hall bar and film stacking. (b) Hall resistance R_H as a function of z -direction external magnetic field H_z in the Pt/Ir/Co system with different Ir thicknesses t_{Ir} , which exhibits a good PMA. (c) R_H and (d) perpendicular magnetic anisotropy field H_k as a function of t_{Ir} in Pt/Ir/Co and PtCr/Ir/Co systems. The curves in Fig. 1(c) represent the curve fitting of the data points. Some error bars, which are not shown in the figure, are smaller than the symbol sizes.

constant indicate the Pt/Co and Ir/Co interfacial DMIs have the same sign and similar magnitude. SOT switching measurements indicate that the Ir insertion layer is able to reduce the switching current density by about 50% at optimal Ir thickness. The simultaneous achievements of lower resistivity, enhanced SOT efficiency, tunable DMI intensity, and decreased switching current density would be technologically important for the development of low-power and high-performance spintronic devices.

II. EXPERIMENTAL

The samples in this work comprise two series multilayer structures: (i) Pt/Ir/Co: Ta(1)/Pt(5.5)/Ir(x)/Co(0.9)/Pt(0.2)/MgO(2)/Ta(1.5) and (ii) PtCr/Ir/Co: Ta(1)/Pt_{0.8}Cr_{0.2}(5)/Pt(0.5)/Ir(x)/Co(0.9)/Pt(0.2)/MgO(2)/Ta(1.5) (the numbers in brackets are in nm) with x ranges from 0–3 nm. All the multilayers were grown on thermally oxidized Si/SiO₂ substrates via AJA magnetron sputtering at room temperature. The base vacuum for magnetron sputtering is better than 3×10^{-5} mtorr, and the working argon pressure is 3 mtorr. The sputtering rate of each layer is calculated by x-ray reflection (XRR). After depositing the films, the actual and nominal values of the film thickness was verified using XRR (see Fig. S1 of the Supplemental Material [33]).

The bottom Ta(1) is to enhance adhesion and make the upper layers more uniform. The Pt(0.5) sandwiched by PtCr

and Ir as well as the Pt(0.2) adjacent to Co(0.9) are intended to enhance the PMA while having little effect on the SOT efficiency. Note that if Pt(0.5) is not inserted, the PtCr/Ir(0.5)/Co possesses very weak PMA and the Pt(0.5) insertion layer is considered to enhance the PMA only (Fig. S2 [33]). The intention of the top MgO(2)/Ta(1.5) is to protect the film from oxidation and simplify the spin current in the system. The Pt_{0.8}Cr_{0.2} layer was sputtered by cosputtering pure Pt and Cr targets, the subscripts represent the atomic ratios of the two elements. According to previous studies [34], 20% Cr has the largest dampinglike effective field when varying the content of Cr, therefore, we concentrate on the effect of the Ir insertion layer in Pt_{0.8}Cr_{0.2}/Ir/Co.

Vibrating sample magnetometer (VSM) was used to examine the magnetism of films. The film was patterned into 5 μ m width Hall bars using a standard photolithography technique, followed by argon ion etching. Then, a secondary photolithography and a lift-off process were undertaken to fabricate the contact electrode Cr(5 nm)/Au(80 nm). It should be noted that the MgO becomes conductive if Ta is on top of it and the metal electrode Cr/Au has a large contact area with Hall bar so that the top MgO/Ta does not affect the electrical transport test. The main stacking structure and measurement scheme of the Hall bar is illustrated in Fig. 1(a). All electrical transport tests were performed in a three-dimensional cryogenic superconducting magnet. The anomalous Hall voltage was measured by applying an ac current in the x direction of

the device and reading the voltage in the y direction while applying a varying magnetic field in the z direction. Current-induced magnetization switching was determined by applying a pulsed current of varying amplitude with a pulse width of 30 μs , after 4 s, the Hall resistance R_H was recorded by a small excitation current. See more measurement details in Supplemental Material [33].

III. RESULTS AND DISCUSSION

A. Modulation of perpendicular magnetic anisotropy

Figure 1(b) describes several prototypical hysteresis loops in Pt/Ir/Co with various Ir thickness. Two important characteristics emerge: first, the Hall resistance (R_H) exhibits a gradual decrease as Ir thickness increases; second, the coercivity field (H_c) initially declines before ascending, with a minimum at $t_{\text{Ir}} = 0.4$ nm. Furthermore, the hysteresis loops suggest robust PMA for all samples, attributable to additional PMA at the Ir/Co interface [19,35]. The R_H attenuation with increasing Ir thickness arises from the parallel shunt effect of the Ir layer as depicted in Fig. 1(c). Interestingly, R_H is roughly inversely proportional to t_{Ir} as described by the curve in Fig. 1(c). To discern the resistivity of each layer, Fig. S3 renders the longitudinal resistance (R_{xx}) for all samples (see Fig. S3 in Supplemental Material [33]). Subsequently, the resistivity of Pt or Pt_{0.8}Cr_{0.2} layer was extracted by subtracting the conductance of control stacks (without Pt or Pt_{0.8}Cr_{0.2}) from the whole stacks, which is consistent with measuring the resistivity of Pt_xCr_{1-x} single layer [34]. The resistivities of the Pt and Pt_{0.8}Cr_{0.2} layers are 36.3 ($\mu\Omega\text{cm}$) and 60.1 ($\mu\Omega\text{cm}$), respectively, which is close to the prior reports [34]. The increase in resistivity makes the R_H of the PtCr/Ir/Co samples larger than that of the Pt/Ir/Co [Fig. 1(c)].

To rationalize the nonmonotonic relationship of H_c , we analyze the perpendicular magnetic anisotropy field (H_k) as a function of t_{Ir} , since H_c and H_k share congruous trends based on our previous study [36]. An in-plane external magnetic field parallel to the current was applied to the device, and a representative plot is shown in Fig. S4 in Supplemental Material [33]. H_k is determined as the spot where the normalized component of the in-plane magnetization $m_x = \sqrt{(1 - m_z^2)}$ reaches 0.98 [37]. In Fig. 1(d), H_k first gradually decreases when $t_{\text{Ir}} = 0-0.4$ nm, experiences a valley at $t_{\text{Ir}} = 0.4-0.5$ nm, then increases at $t_{\text{Ir}} = 0.5-1.0$ nm and saturates at $t_{\text{Ir}} = 1.0-3.0$ nm. This signature persists irrespective of a Pt or PtCr heavy-metal layer, implicating an intrinsic attribute of the Ir interlayer. Another phenomenon is that the H_k of Pt-based is larger than Pt/Cr-based devices with different Ir thickness [34]. The collective evidence points to substantive PMA modulation by the Ir insertion layer. The mechanistic explanation of H_k as a function of Ir thickness will be elaborated in Sec. III C, primarily stemming from interfacial roughness effect.

B. Enhancement of spin-orbit torque efficiency

Next, the hysteresis loop shift method based on chiral domain wall was employed to accurately measure charge-spin conversion efficiency [38,39]. As illustrated in Fig. 2(a), the anomalous Hall voltage shift with respect to the out-of-plane

magnetic field (H_z) was measured under dc current and in-plane bias field (H_x). A representative normalized hysteresis loop shift for PtCr/Pt(0.5)/Ir(0)/Co is depicted in Fig. 2(a). The loop shifts left (right) when +2 mA (-2 mA) is applied at $H_x = 1000$ Oe, indicating current-induced dampinglike torque drove magnetic domain wall motion [38]. This opposite horizontal movement is attributed to the dampinglike effective field (H_z^{eff}) along z generated by SOT, the magnitude of which scales linearly with dc current, and the sign depends on the bias field direction as shown in Fig. 2(b). The excellent linear relationship between H_z^{eff} and I_{dc} suggests negligible Joule heating due to the relatively small I_{dc} , allowing us to easily get the slope of H_z^{eff} vs I_{dc} . Next, the $H_z^{\text{eff}}/I_{\text{dc}}$ of this sample was characterized at different bias fields as depicted in Fig. 2(c). As H_x increases, the slope rises and saturates when $H_x > H_{\text{DMI}}$, allowing simultaneous quantification of DMI field and SOT efficiency.

Considering the shunting effect of each layer, the SOT effective field per unit current density is defined as: $\beta_{\text{DL}} = H_z^{\text{eff}}/J$. The dampinglike SOT efficiency is calculated as [20,40]: $\xi_{\text{DL}} = (2e/\hbar)(2/\pi)\mu_0 M_s t_{\text{FM}} H_{z(\text{sat})}^{\text{eff}}/(J)$, where μ_0 , M_s , and t_{FM} represent vacuum permeability, saturation magnetization, and ferromagnetic thickness, respectively. The VSM show that $M_s = 1200$ (emu/cm^3) as shown in Fig. S5 in Supplemental Material [33], in particular the M_s hardly varies with the thickness of the inserted Ir layer [19]. As summarized in Fig. 2(d), when $t_{\text{Ir}} = 0$ nm, $\beta_{\text{DL}} = 6.2$, and 11.8 [$\text{Oe}/(10^6 \text{A}/\text{cm}^2)$] for Pt/Ir(0)/Co and PtCr/Pt(0.5)/Ir(0)/Co, corresponding to $\xi_{\text{DL}} = 0.13$ and 0.246, respectively. The higher efficiency of PtCr arises from balanced intrinsic spin Hall conductivity of Pt and the spin-carrier lifetime [34]. With the thickness of Ir is about one atomic layer ($t_{\text{Ir}} = 0.1-0.3$ nm), it is noteworthy that ξ_{DL} of Pt/Ir(0.1)/Co increases 26% to 0.164, attributed to additional impurity scattering, which may be similar to the Pt/Hf and Pt/Ti multilayers [41,42]. Similarly, the SOT efficiency ξ_{DL} rises 10% to 0.271 for PtCr/Pt(0.5)/Ir(0.1)/Co, less than Pt/Ir/Co due to existing alloy scattering in PtCr. The direct evidence for the enhancement of impurity scattering is the slight enhancement of the resistivity R_{xx} at $t_{\text{Ir}} = 0.1$ nm [43]. Since the spin Hall angle of Ir is only about 0.014-0.02 [19,44], which is much smaller than that of Pt. And Pt, Pt_{0.8}Cr_{0.2}, and Ir have comparable spin diffusion lengths of 1.4 nm [45], 1.6 nm [34], and 1.35 nm [19], respectively. It can be inferred that the spin flow generated from Pt is continuously dissipated in the Ir layer with the increase of the Ir thickness. As stated in Fig. 2(d), the dampinglike SOT efficiency of the system gradually decreases and tends to stabilize when the thickness of Ir is increased to 3 nm, $\xi_{\text{DL}} = 0.078$ for PtCr/Pt(0.5)/Ir(3)/Co and $\xi_{\text{DL}} = 0.048$ for Pt/Ir(3)/Co. However, the value of the SOT efficiency is slightly larger than the spin Hall angle of Ir, indicating that a portion of the spin flow is still supplied by Pt at $t_{\text{Ir}} = 3$ nm.

C. Tunable DMI interaction strength

As mentioned previously, the DMI effective field (H_{DMI}) can be determined from the saturation bias field of the hysteresis loop shift. H_{DMI} as a function of Ir thickness for Pt/Ir/Co

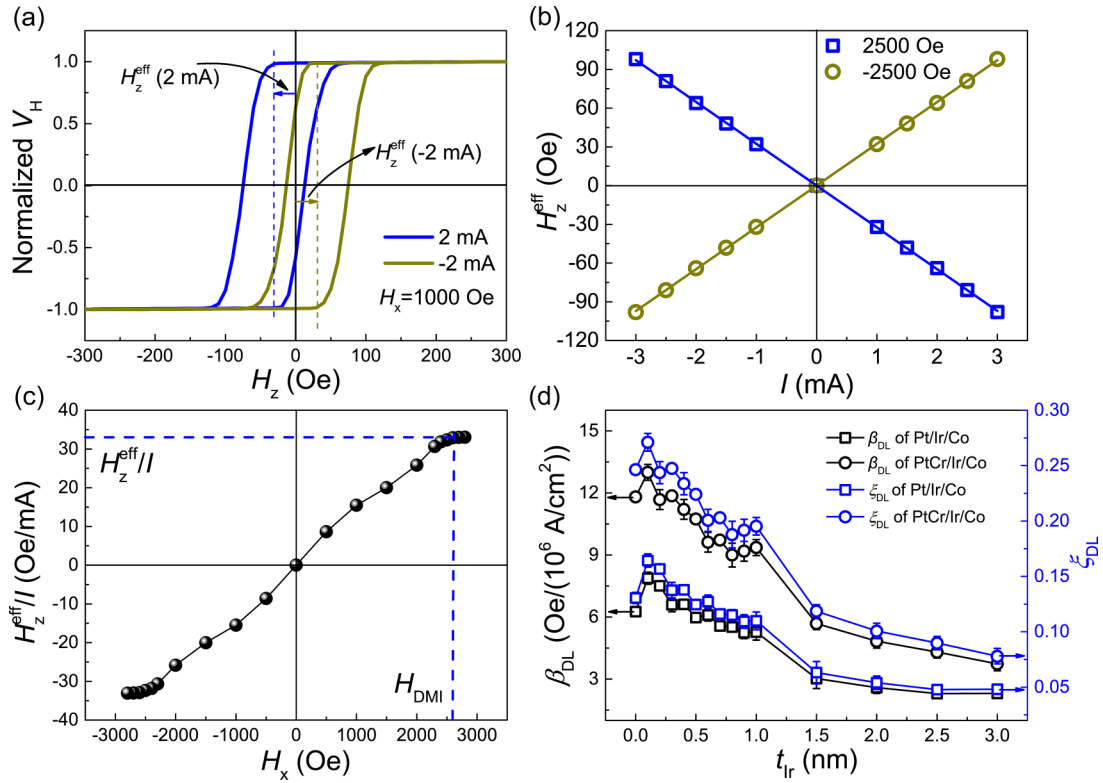


FIG. 2. (a) Representative normalized anomalous Hall loops for the PtCr/Pt(0.5)/Ir(0)/Co structure when the in-plane bias field $H_x = 1000$ Oe and the applied dc current is ± 2 mA. H_z^{eff} represents the offset of the anomalous Hall loop due to the spin Hall effect. (b) H_z^{eff} as a linear function of the dc current magnitude at $H_x = \pm 2500$ Oe for PtCr/Pt(0.5)/Ir(0)/Co structure. (c) The measured H_z^{eff} per mA versus H_x . The DMI effective field H_{DMI} and saturated H_z^{eff}/I can also be extracted from the figure. (d) β_{DL} and ξ_{DL} as a function of t_{Ir} in Pt/Ir/Co and PtCr/Ir/Co systems. Some error bars, which are not shown in the figure, are smaller than the symbol sizes.

and PtCr/Ir/Co is shown in Fig. 3(a). Similar to H_k , H_{DMI} of the two systems also first decreases at $t_{\text{Ir}} = 0-0.4$ nm, then increases at $t_{\text{Ir}} = 0.5-1$ nm, and finally saturates at $t_{\text{Ir}} = 1-3$ nm. The magnitude of H_{DMI} is close for $t_{\text{Ir}} = 0$ and $t_{\text{Ir}} = 3$ nm. Furthermore, The DMI exchange constant $|D|$ can be calculated through [38,46]: $|D| = \mu_0 M_S (A/K_u)^{1/2} |H_{\text{DMI}}|$, where A is exchange stiffness constant around 1.5×10^{11} (J/m) [47],

effective magnetic anisotropy $K_u = (1/2)\mu_0 M_S H_k$ [19]. In Fig. S6, a tunable $|D|$ is presented for both Pt/Ir/Co and PtCr/Ir/Co systems, which is comparable to Pt/Co systems [48,49] (see Fig. S6 in Supplemental Material [33]). The DMI exchange constant, which can be tuned from a maximum of 3.3 to 1.5 (mJ/m²) in the two systems, highlights the interesting nature of the Ir insertion layer.

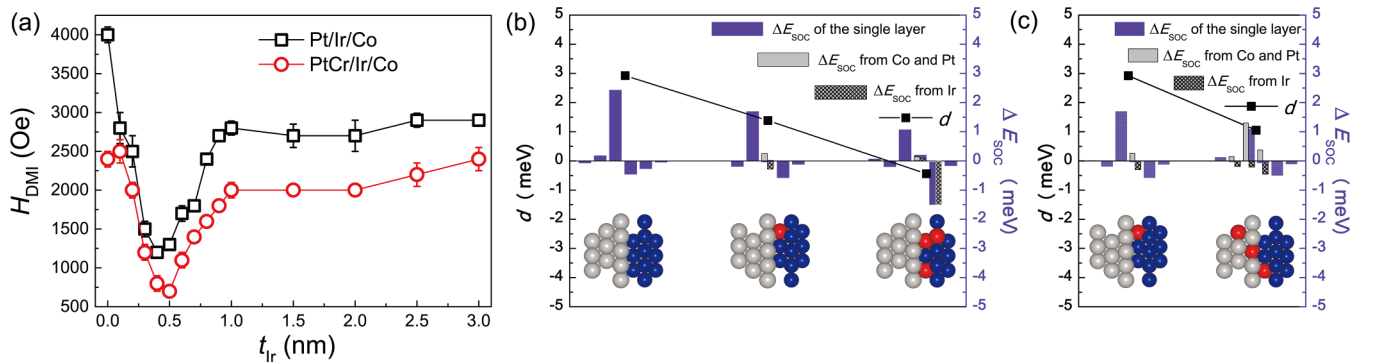


FIG. 3. (a) DMI effective field H_{DMI} as a function of Ir thickness in Pt/Ir/Co and PtCr/Ir/Co systems. Some error bars, which are not shown in the figure, are smaller than the symbol sizes. The calculated total DMI (black line) and layer-resolved SOC energy difference ΔE_{SOC} between ACW and CW chirality of Pt/Co heterostructures with different roughness induced by random Ir substitution. (b) The roughness exists only in Co layers and (c) the case that the roughness also exists in Pt layers. The positive and negative d values represent the ACW and CW chirality, respectively. The gray, blue, and red balls represent Pt, Co, and Ir atoms, correspondingly. The violet bars show the ΔE_{SOC} from the whole single layer. The gray bars display the ΔE_{SOC} from the Co and Pt atoms in the single layer, and the gray bars with dense crossing patterns are ΔE_{SOC} from Ir atoms in the single layer.

Then, we will explain the nonmonotonic relationship of H_k and H_{DMI} . First, H_{DMI} is defined as the threshold required to just exceed the stabilizing chiral domain wall, and H_{DMI} and H_k have the following correspondence: $H_{\text{DMI}}/H_k = 2/\pi$ [46], as proved in Fig. S7 in Supplemental Material [33]. Second, the DMI interaction at the Pt/Co interface is close in magnitude and of the same sign as the Ir/Co interface [22,23,30,50–52]. Based on those, when there is no Ir insertion layer, Pt/Co interface is responsible for the PMA and DMI. However, when a thin Ir is inserted ($t_{\text{Ir}} < 0.5$ nm), it can be inferred that the Ir insertion into the Pt/Co interface causes a large interfacial roughness, which disrupts the Pt/Co interface, yet does not form a stable Ir/Co interface, and thus reduces the PMA and DMI. The aforementioned interfacial roughness can be verified from experiment and the first-principles calculation. In experiment, a significant enhancement of the perpendicular magnetic anisotropy was observed by sputtering the same film [Pt/Ir(0.5)/Co] at high temperature (350 °C) (Fig. S8 [33]), since high-temperature sputtering can cause the atomic relaxation, thereby ordering the striped domains [53].

The influence of interfacial roughness on the DMI in a Co/Pt multilayer structure is investigated using first-principles calculations (Fig. S9 [33]). Heterostructures with varying interfacial roughness are constructed by randomly substituting Co and Pt atoms with Ir in a 2×2 supercell. The DMI constant d is calculated using the chirality-dependent total energy difference approach, which has been successfully utilized for Co/Pt films previously [54]. As interfacial roughness induced by Ir substitution increases, the value of d gradually decreases [Figs. 3(b) and 3(c)]. High Ir substitution can even reverse the chirality of the pristine Co/Pt film from anticlockwise (ACW) to clockwise (CW). To elucidate the mechanism behind the evolution of interfacial DMI, layer-resolved localization of the DMI-associated spin-orbit coupling energy ΔE_{SOC} is analyzed. For original Co/Pt films with crystalline Pt/Co interfaces, substantial DMI between Co spins arises due to spin-orbital scattering of conduction electrons by neighboring Pt atoms (the largest correlated ΔE_{SOC} originates from adjacent Pt layers). This agrees with the Fert-Levy model of interfacial DMI. The disorder introduced by Ir substitution disrupts the Co-Co-Pt triplet and reduces the energy contribution from the Pt layer. Additionally, disordered Ir atoms provide ΔE_{SOC} with opposite CW chirality, counteracting the ACW ΔE_{SOC} from Pt atoms. The case that the substitution of Pt atoms is also considered. As shown in Fig. 3(c), the ΔE_{SOC} from the Ir atoms in the Pt layer has CW chirality, which can cancel out the ACW ΔE_{SOC} from Pt atoms and reduce the total DMI. Consequently, the total interfacial DMI is diminished as interfacial roughness increases due to Ir substitution. Thus, the combined results of experiments and first principles confirm that roughness plays a decisive role in the decrease of H_k and H_{DMI} [55]. However, when the thickness of Ir is relatively thick ($t_{\text{Ir}} = 1\text{--}3$ nm), the PMA and DMI are ascribed to the Ir/Co interface. Besides, the fact that H_k has the close value at $t_{\text{Ir}} = 0$ nm and 3 nm confirms the equivalence of the intensity of the DMI interaction at the Pt/Co and Ir/Co interfaces.

Furthermore, we use atomic force microscopy (AFM) and XRR to characterize the roughness as Ir thickness

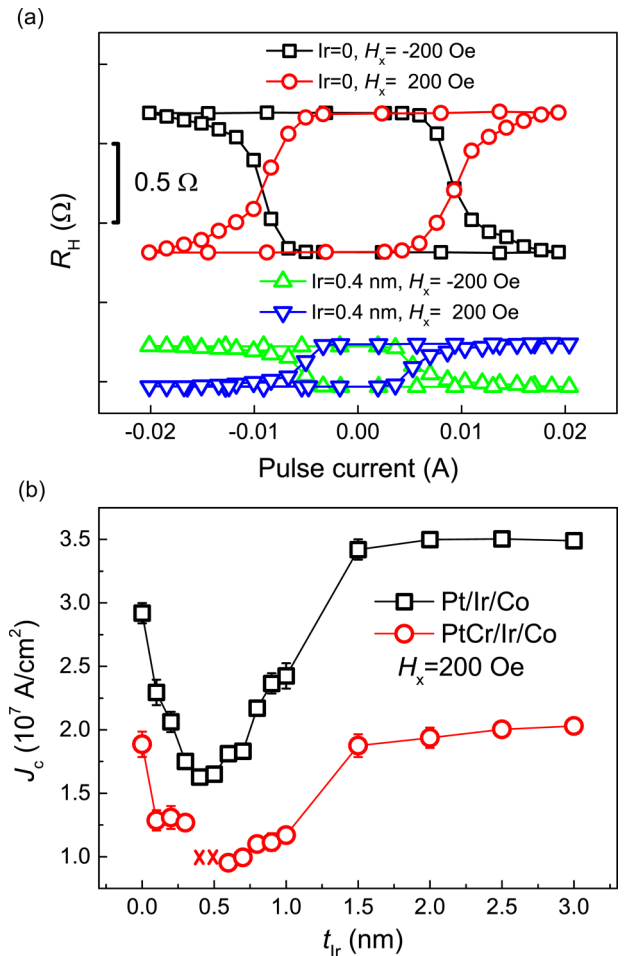


FIG. 4. (a) Current-induced magnetization switching at an in-plane auxiliary field of ± 200 Oe for the Pt/Ir/Co system with different Ir thicknesses (0 and 0.4 nm), the figure also reveals the scale. (b) Critical switching current density as a function of Ir thickness in Pt/Ir/Co and PtCr/Ir/Co systems after considering shunt effects. The crosses represent the inability to switching due to weak anisotropy. Some error bars, which are not shown in the figure, are smaller than the symbol sizes.

varies. AFM shows that the average roughness of all the films is very low (Fig. S10 [33]). Then we measure the interfacial roughness of Ir using simplified film stacks [Ta(15)/Pt(5.5)/Ir(0.5)/Au(10) and Ta(15)/Pt(5.5)/Ir(3)/Au(10)] (Fig. S11 [33]). The results show that the roughness of Ir layer at $t_{\text{Ir}} = 0.5$ nm was larger than that of $t_{\text{Ir}} = 3$ nm (Table S1 [33]), providing a direct evidence for the reduced roughness as Ir thickness increases.

D. Current-induced magnetization switching

Next, we investigated current-driven SOT switching for the two systems. A small in-plane auxiliary magnetic field is applied collinear to the charge current to break the mirror symmetry. A reduction of the critical switching current density will be foreseen when the H_{DMI} decreases and can be verified from Fig. 4(a). The critical switching current is defined as the current at which 50% magnetization is switched. When

$H_x = 200$ Oe, the critical switching current is 9.4 mA and 5.6 mA, corresponding to Pt/Co and Pt/Ir(0.4)/Co, respectively, which throws light on the viability of modulating the interfacial DMI effective field and reducing the critical switching current density through Ir insertion for energy-efficient spintronic devices.

Additionally, we describe the relationship between the critical switching current density and the Ir thickness in the two systems. As demonstrated in Fig. 4(b), the critical switching current density for both systems initially decreases from $t_{\text{Ir}} = 0$ –0.5 nm, then increases within $t_{\text{Ir}} = 0.5$ –1.5 nm, and finally reaches a plateau. The critical switching current density can be drastically adjusted from 1.6 – 3.5×10^7 (A/cm²) in Pt/Ir/Co and 1.0 – 2.0×10^7 (A/cm²) in PtCr/Ir/Co, respectively. For PtCr/Pt(0.5)/Ir(0.4–0.5 nm)/Co, due to the weak anisotropy, we use crosses to indicate its inability to switch magnetization. This trend aligns with the DMI variations, substantiating that attenuated DMI facilitates reduced SOT critical switching current density. Furthermore, the critical switching current density of the PtCr/Ir/Co system is 1.5–1.8 times greater than that of Pt/Ir/Co, analogous to the SOT efficiency ratio in Fig. 2(d). Hence, intercalating Ir between the Pt or PtCr/Pt(0.5) and Co layers engenders tunable critical switching current density across a wide range, underscoring prospects for reduced energy consumption in spintronic devices by means of interface DMI engineering.

IV. CONCLUSIONS

In conclusion, the insertion of an ultrathin 0.1 nm Ir layer led to a remarkable enhancement of over 26% and

10% in the dampinglike SOT efficiency for the Pt/Co and PtCr/Co systems, respectively. This enhancement stems from increased interfacial impurity scattering induced by the Ir insertion layer. The perpendicular magnetic anisotropy and Dzyaloshinskii-Moriya interaction were found to vary non-monotonically with Ir thickness, minimized at 0.4–0.5 nm thickness. Using first-principles calculations, this trend could be attributed to interfacial roughness effects introduced by Ir insertion. The critical switching current density became widely tunable from 1.6 – 3.5×10^7 (A/cm²) in Pt/Ir/Co and 1.0 – 2.0×10^7 (A/cm²) in PtCr/Ir/Co, respectively, by modulating the Dzyaloshinskii-Moriya interaction strength through the Ir layer thickness. A nearly 50% reduction in switching current was achieved with a 0.4 nm Ir insertion. The capability to substantially enhance the SOT efficiency while reducing the switching current highlights the exceptional promise of an Ir insertion layer for unlocking the full potential of spin-orbit torque-based spintronic devices. By providing pivotal insights into interfacial spin-orbit coupling effects and interface engineering, this work lays the foundation for optimization of next-generation spin-orbitronics.

ACKNOWLEDGMENTS

This work was supported by the “Pioneer” and “Leading Goose” R&D Program of Zhejiang Province under Grant No. 2022C01053, Key Research and Development Program of Zhejiang Province (Grant No. 2021C01039), National Natural Science Foundation of China (Grant No. 62293493), Natural Science Foundation of Zhejiang Province, China (Grant No. LQ21A050001).

-
- [1] Q. Shao, P. Li, L. Liu, H. Yang, S. Fukami, A. Razavi, H. Wu, K. Wang, F. Freimuth, Y. Mokrousov *et al.*, Roadmap of spin-orbit torques, *IEEE Trans. Magn.* **57**, 800439 (2021).
 - [2] C. Song, R. Zhang, L. Liao, Y. Zhou, X. Zhou, R. Chen, Y. You, X. Chen, and F. Pan, Spin-orbit torques: Materials, mechanisms, performances, and potential applications, *Prog. Mater. Sci.* **118**, 100761 (2021).
 - [3] A. Manchon, J. Železný, I. M. Miron, T. Jungwirth, J. Sinova, A. Thiaville, K. Garello, and P. Gambardella, Current-induced spin-orbit torques in ferromagnetic and antiferromagnetic systems, *Rev. Mod. Phys.* **91**, 035004 (2019).
 - [4] H. Wu, J. Zhang, B. Cui, S. A. Razavi, X. Che, Q. Pan, D. Wu, G. Yu, X. Han, and K. L. Wang, Field-free approaches for deterministic spin-orbit torque switching of the perpendicular magnet, *Mater. Futures* **1**, 022201 (2022).
 - [5] I. M. Miron, K. Garello, G. Gaudin, P.-J. Zermatten, M. V. Costache, S. Auffret, S. Bandiera, B. Rodmacq, A. Schuhl, and P. Gambardella, Perpendicular switching of a single ferromagnetic layer induced by in-plane current injection, *Nature (London)* **476**, 189 (2011).
 - [6] L. Liu, C.-F. Pai, Y. Li, H. Tseng, D. Ralph, and R. Buhrman, Spin-torque switching with the giant spin Hall effect of tantalum, *Science* **336**, 555 (2012).
 - [7] L. Liu, O. J. Lee, T. J. Gudmundsen, D. C. Ralph, and R. A. Buhrman, Current-induced switching of perpendicularly magnetized magnetic layers using spin torque from the spin Hall effect, *Phys. Rev. Lett.* **109**, 096602 (2012).
 - [8] P. Haazen, E. Murè, J. Franken, R. Lavrijsen, H. Swagten, and B. Koopmans, Domain wall depinning governed by the spin Hall effect, *Nature Mater.* **12**, 299 (2013).
 - [9] S. Emori, U. Bauer, S.-M. Ahn, E. Martinez, and G. S. Beach, Current-driven dynamics of chiral ferromagnetic domain walls, *Nature Mater.* **12**, 611 (2013).
 - [10] W. Jiang, P. Upadhyaya, W. Zhang, G. Yu, M. B. Jungfleisch, F. Y. Fradin, J. E. Pearson, Y. Tserkovnyak, K. L. Wang, O. Heinonen *et al.*, Blowing magnetic skyrmion bubbles, *Science* **349**, 283 (2015).
 - [11] T. Jungwirth, J. Wunderlich, and K. Olejník, Spin Hall effect devices, *Nature Mater.* **11**, 382 (2012).
 - [12] J. Sinova, S. O. Valenzuela, J. Wunderlich, C. H. Back, and T. Jungwirth, Spin Hall effects, *Rev. Mod. Phys.* **87**, 1213 (2015).
 - [13] Q. Shao, G. Yu, Y.-W. Lan, Y. Shi, M.-Y. Li, C. Zheng, X. Zhu, L.-J. Li, P. K. Amiri, and K. L. Wang, Strong Rashba-Edelstein effect-induced spin-orbit torques in monolayer transition metal dichalcogenide/ferromagnet bilayers, *Nano Lett.* **16**, 7514 (2016).
 - [14] Y. Du, H. Gamou, S. Takahashi, S. Karube, M. Kohda, and J. Nitta, Disentanglement of spin-orbit torques in Pt/Co bilayers with the presence of spin Hall effect and Rashba-Edelstein effect, *Phys. Rev. Appl.* **13**, 054014 (2020).

- [15] L. Zhu, D. C. Ralph, and R. A. Buhrman, Maximizing spin-orbit torque generated by the spin Hall effect of Pt, *Appl. Phys. Rev.* **8**, 031308 (2021).
- [16] C. O. Avci, G. S. D. Beach, and P. Gambardella, Effects of transition metal spacers on spin-orbit torques, spin Hall magnetoresistance, and magnetic anisotropy of Pt/Co bilayers, *Phys. Rev. B* **100**, 235454 (2019).
- [17] S. Li, X. Zhao, W. Liu, X. Zhao, and Z. Zhang, Modulation of spin-orbit torque induced magnetization switching in Pt/CoFe through oxide interlayers, *Appl. Phys. Lett.* **114**, 212404 (2019).
- [18] L. Zhu, L. Zhu, and R. A. Buhrman, Fully spin-transparent magnetic interfaces enabled by the insertion of a thin paramagnetic NiO layer, *Phys. Rev. Lett.* **126**, 107204 (2021).
- [19] X. Luo, X. Wang, J. Wei, W. Yang, M. Zhao, Y. Wang, Y. Wang, W. He, B. He, Z. Zeng *et al.*, Modulation of spin-orbit torque and large enhancement of perpendicular magnetic anisotropy in W/Co₂₀Fe₆₀B₂₀/MgO by Ir insertion layer, *Phys. Rev. Appl.* **19**, 034043 (2023).
- [20] M.-H. Nguyen, C.-F. Pai, K. X. Nguyen, D. A. Muller, D. C. Ralph, and R. A. Buhrman, Enhancement of the anti-damping spin torque efficacy of platinum by interface modification, *Appl. Phys. Lett.* **106**, 222402 (2015).
- [21] M. Mann and G. Beach, Reduction of in-plane field required for spin-orbit torque magnetization reversal by insertion of Au spacer in Pt/Au/Co/Ni/Co/Ta, *APL Mater.* **5**, 106104 (2017).
- [22] D. Khadka, S. Karayev, and S. Huang, Dzyaloshinskii–Moriya interaction in Pt/Co/Ir and Pt/Co/Ru multilayer films, *J. Appl. Phys.* **123**, 123905 (2018).
- [23] K. Shahbazi, J.-V. Kim, H. T. Nembach, J. M. Shaw, A. Bischof, M. D. Rossell, V. Jeudy, T. A. Moore, and C. H. Marrows, Domain-wall motion and interfacial Dzyaloshinskii–Moriya interactions in Pt/Co/Ir(t_{Ir})/Ta multilayers, *Phys. Rev. B* **99**, 094409 (2019).
- [24] Y. Ishikuro, M. Kawaguchi, N. Kato, Y.-C. Lau, and M. Hayashi, Dzyaloshinskii–Moriya interaction and spin-orbit torque at the Ir/Co interface, *Phys. Rev. B* **99**, 134421 (2019).
- [25] A. van den Brink, G. Vermijs, A. Solignac, J. Koo, J. T. Kohlhepp, H. J. Swagten, and B. Koopmans, Field-free magnetization reversal by spin-Hall effect and exchange bias, *Nat. Commun.* **7**, 10854 (2016).
- [26] Y.-W. Oh, S.-h. Chris Baek, Y. Kim, H. Y. Lee, K.-D. Lee, C.-G. Yang, E.-S. Park, K.-S. Lee, K.-W. Kim, G. Go *et al.*, Field-free switching of perpendicular magnetization through spin-orbit torque in antiferromagnet/ferromagnet/oxide structures, *Nat. Nanotechnol.* **11**, 878 (2016).
- [27] S. A. Razavi, D. Wu, G. Yu, Y.-C. Lau, K. L. Wong, W. Zhu, C. He, Z. Zhang, J. M. D. Coey, P. Stamenov, P. KhaliliAmiri, and K. L. Wang, Joule heating effect on field-free magnetization switching by spin-orbit torque in exchange-biased systems, *Phys. Rev. Appl.* **7**, 024023 (2017).
- [28] H. Fan, M. Jin, B. Wu, M. Wei, J. Wang, Z. Shao, C. Yu, J. Wen, H. Li, W. Li, *et al.*, Field-free switching and high spin-orbit torque efficiency in Co/Ir/CoFeB synthetic antiferromagnets deposited on miscut Al₂O₃ substrates, *Appl. Phys. Lett.* **122**, 262404 (2023).
- [29] Q. Ma, Y. Li, Y.-s. Choi, W.-C. Chen, S. J. Han, and C. Chien, Spin orbit torque switching of synthetic Co/Ir/Co trilayers with perpendicular anisotropy and tunable interlayer coupling, *Appl. Phys. Lett.* **117**, 172403 (2020).
- [30] Y. Saito, S. Ikeda, and T. Endoh, Enhancement of current to spin-current conversion and spin torque efficiencies in a synthetic antiferromagnetic layer based on a Pt/Ir/Pt spacer layer, *Phys. Rev. B* **105**, 054421 (2022).
- [31] Y. Saito, N. Tezuka, S. Ikeda, and T. Endoh, Antiferromagnetic interlayer exchange coupling and large spin Hall effect in multilayer systems with Pt/Ir/Pt and Pt/Ir layers, *Phys. Rev. B* **104**, 064439 (2021).
- [32] R. Q. Zhang, L. Y. Liao, X. Z. Chen, H. Q. Wu, F. Pan, and C. Song, Strong magnetoresistance modulation by Ir insertion in a Ta/Ir/CoFeB trilayer, *Phys. Rev. B* **100**, 144425 (2019).
- [33] See Supplemental Material at <http://link.aps.org/supplemental/10.1103/PhysRevB.108.224409> for the measurement details, XRR measurement of the sample, the effect of Pt(0.5) on the magnetic moment and coercivity, longitudinal resistance R_{xx} , test method of H_k , VSM measurement of the sample, DMI exchange constant, the relationship between H_{DMI} and H_k , enhancement of H_k through high-temperature deposited, first-principles calculation methods and schematic heterostructure, interface roughness characterization. It also contains Refs. [49,54,56–61].
- [34] Q. Liu, J. Li, L. Zhu, X. Lin, X. Xie, and L. Zhu, Strong spin-orbit torque induced by the intrinsic spin Hall effect in Cr_{1-x}Pt_x, *Phys. Rev. Appl.* **18**, 054079 (2022).
- [35] K. Yakushiji, H. Kubota, A. Fukushima, and S. Yuasa, Perpendicular magnetic tunnel junction with enhanced anisotropy obtained by utilizing an Ir/Co interface, *Appl. Phys. Express* **9**, 013003 (2015).
- [36] H. Fan, Y. Luo, B. Wu, X. Xu, Y. Zhuang, Z. Feng, W. Li, and T. Zhou, Enhancement of damping-like field and field-free switching in Co/Pt bilayer films through quantitative engineering of anisotropy gradient, *Appl. Phys. Lett.* **120**, 142401 (2022).
- [37] A. Razavi, H. Wu, B. Dai, H. He, D. Wu, K. Wong, G. Yu, and K. L. Wang, Spin-orbit torques in structures with asymmetric dusting layers, *Appl. Phys. Lett.* **117**, 182403 (2020).
- [38] C.-F. Pai, M. Mann, A. J. Tan, and G. S. D. Beach, Determination of spin torque efficiencies in heterostructures with perpendicular magnetic anisotropy, *Phys. Rev. B* **93**, 144409 (2016).
- [39] T. C. Chuang, C. F. Pai, and S. Y. Huang, Cr-induced perpendicular magnetic anisotropy and field-free spin-orbit-torque switching, *Phys. Rev. Appl.* **11**, 061005(R) (2019).
- [40] C.-F. Pai, Y. Ou, L. H. Vilela-Leão, D. C. Ralph, and R. A. Buhrman, Dependence of the efficiency of spin Hall torque on the transparency of Pt/ferromagnetic layer interfaces, *Phys. Rev. B* **92**, 064426 (2015).
- [41] L. Zhu, L. Zhu, S. Shi, M. Sui, D. C. Ralph, and R. A. Buhrman, Enhancing spin-orbit torque by strong interfacial scattering from ultrathin insertion layers, *Phys. Rev. Appl.* **11**, 061004(R) (2019).
- [42] L. Zhu and R. A. Buhrman, Maximizing spin-orbit-torque efficiency of Pt/Ti multilayers: Trade-off between intrinsic spin Hall conductivity and carrier lifetime, *Phys. Rev. Appl.* **12**, 051002(R) (2019).
- [43] L. Zhu, K. Sobotkiewicz, X. Ma, X. Li, D. C. Ralph, and R. A. Buhrman, Strong damping-like spin-orbit torque and tunable Dzyaloshinskii–Moriya interaction generated by low-resistivity Pd_{1-x}Pt_x alloys, *Adv. Funct. Mater.* **29**, 1805822 (2019).
- [44] T. Fache, J. C. Rojas-Sanchez, L. Badie, S. Mangin, and S. Petit-Watelot, Determination of spin Hall angle, spin

- mixing conductance, and spin diffusion length in CoFeB/Ir for spin-orbitronic devices, *Phys. Rev. B* **102**, 064425 (2020).
- [45] L. Liu, T. Moriyama, D. C. Ralph, and R. A. Buhrman, Spin-torque ferromagnetic resonance induced by the spin Hall effect, *Phys. Rev. Lett.* **106**, 036601 (2011).
- [46] A. Thiaville, S. Rohart, É. Jué, V. Cros, and A. Fert, Dynamics of Dzyaloshinskii domain walls in ultrathin magnetic films, *Europhys. Lett.* **100**, 57002 (2012).
- [47] P. J. Metaxas, J. P. Jamet, A. Mougin, M. Cormier, J. Ferré, V. Baltz, B. Rodmacq, B. Dieny, and R. L. Stamps, Creep and flow regimes of magnetic domain-wall motion in ultrathin Pt/Co/Pt films with perpendicular anisotropy, *Phys. Rev. Lett.* **99**, 217208 (2007).
- [48] O. Boulle, J. Vogel, H. Yang, S. Pizzini, D. de Souza Chaves, A. Locatelli, T. O. Mentes, A. Sala, L. D. Buda-Prejbeanu, O. Klein *et al.*, Room-temperature chiral magnetic skyrmions in ultrathin magnetic nanostructures, *Nat. Nanotechnol.* **11**, 449 (2016).
- [49] H. Yang, O. Boulle, V. Cros, A. Fert, and M. Chshiev, Controlling Dzyaloshinskii-Moriya interaction via chirality dependent atomic-layer stacking, insulator capping and electric field, *Sci. Rep.* **8**, 12356 (2018).
- [50] P. M. Shepley, H. Tunncliffe, K. Shahbazi, G. Burnell, and T. A. Moore, Magnetic properties, domain-wall creep motion, and the Dzyaloshinskii-Moriya interaction in Pt/Co/Ir thin films, *Phys. Rev. B* **97**, 134417 (2018).
- [51] N.-H. Kim, J. Jung, J. Cho, D.-S. Han, Y. Yin, J.-S. Kim, H. J. Swagten, and C.-Y. You, Interfacial Dzyaloshinskii-Moriya interaction, surface anisotropy energy, and spin pumping at spin orbit coupled Ir/Co interface, *Appl. Phys. Lett.* **108**, 142406 (2016).
- [52] K.-S. Ryu, S.-H. Yang, L. Thomas, and S. S. Parkin, Chiral spin torque arising from proximity-induced magnetization, *Nat. Commun.* **5**, 3910 (2014).
- [53] L. Tong, P. Deng, X.-M. He, and T. Li, Abnormal effect of substrate temperature on perpendicular magnetic anisotropy in sputter-deposited NdFeCo films on silicon substrates, *Thin Solid Films* **562**, 543 (2014).
- [54] H. Yang, A. Thiaville, S. Rohart, A. Fert, and M. Chshiev, Anatomy of Dzyaloshinskii-Moriya interaction at Co/Pt interfaces, *Phys. Rev. Lett.* **115**, 267210 (2015).
- [55] R. Chen, Q. Cui, L. Liao, Y. Zhu, R. Zhang, H. Bai, Y. Zhou, G. Xing, F. Pan, H. Yang *et al.*, Reducing Dzyaloshinskii-Moriya interaction and field-free spin-orbit torque switching in synthetic antiferromagnets, *Nat. Commun.* **12**, 3113 (2021).
- [56] W. Kohn and L. J. Sham, Self-consistent equations including exchange and correlation effects, *Phys. Rev.* **140**, A1133 (1965).
- [57] G. Kresse and J. Furthmüller, Efficient iterative schemes for *ab initio* total-energy calculations using a plane-wave basis set, *Phys. Rev. B* **54**, 11169 (1996).
- [58] G. Kresse and J. Hafner, *Ab initio* molecular dynamics for liquid metals, *Phys. Rev. B* **47**, 558 (1993).
- [59] G. Kresse and J. Hafner, *Ab initio* molecular-dynamics simulation of the liquid-metal–amorphous-semiconductor transition in germanium, *Phys. Rev. B* **49**, 14251 (1994).
- [60] G. Kresse and J. Furthmüller, Efficiency of *ab initio* total energy calculations for metals and semiconductors using a plane-wave basis set, *Comput. Mater. Sci.* **6**, 15 (1996).
- [61] J. P. Perdew, K. Burke, and M. Ernzerhof, Generalized gradient approximation made simple, *Phys. Rev. Lett.* **77**, 3865 (1996).